12 Mc

AFGL-TR-77-0131

ERROR MODELS FOR PROTOTYPE MOVING-BASE GRAVITY GRADIOMETERS

Warren G. Heller

The Analytic Sciences Corporation
Six Jacob Way
Reading, Massachusetts 01867

30 April 1977

Final Report
1 December 1975 - 30 April 1977

Approved for public release; distribution unlimited

SPONSORED BY
DEFENSE ADVANCED RESEARCH PROJECTS AGENCY (DoD)
ARPA ORDER 2895

AIR FORCE GEOPHYSICS LABORATORY
AIR FORCE SYSTEMS COMMAND
UNITED STATES AIR FORCE
HANSCOM AFB, MASSACHUSETTS 01731

ARPA Order Number 2895	Contract Number 1-19628-76-0079
Program Code Number N/A	Principal Investigator and Phone Number S. K. Jordan (617-944-6850)
Start Date of Contract 12/1/75	RADC Project Engineer and Phone Number N/A
Contract Period Covered by Report 12/1/75 - 4/30/77	Contract Expiration Date 30 June 1977
Short Title of Work Error Models for Gradiometers	Date of Report 30 April 1977

UNCLASSIFIED

SECURITY CLASSIFICATION OF THIS PAGE (When Data Entered)

REPORT DOCUMENTATION PAGE	READ INSTRUCTIONS BEFORE COMPLETING FORM
1. REPORT NUMBER: AFGL-TR-77-0131	2. GOVT ACCESSION NO.: None
3. RECIPIENT'S CATALOG NUMBER:	
4. TITLE (and Subtitle): ERROR MODELS FOR PROTOTYPE MOVING-BASE GRAVITY GRADIOMETERS	5. TYPE OF REPORT & PERIOD COVERED: Final Report. 12/1/75 - 4/30/77
	6. PERFORMING ORG. REPORT NUMBER: TR-823-1
7. AUTHOR(s): Warren G. Heller	8. CONTRACT OR GRANT NUMBER(s): F19628-76-C-0079, ARPA Order-2895
9. PERFORMING ORGANIZATION NAME AND ADDRESS: The Analytic Sciences Corporation, Six Jacob Way, Reading, Massachusetts 01867	10. PROGRAM ELEMENT, PROJECT, TASK AREA & WORK UNIT NUMBERS: PE 62701E, ARPA Order No. 2895, PE62101 F 760006
11. CONTROLLING OFFICE NAME AND ADDRESS: Air Force Geophysics Laboratory, Hanscom AFB, Massachusetts 01731, Monitor/Dr. James A. Hammond/LWG	12. REPORT DATE: 30 April 1977
	13. NUMBER OF PAGES: 51
14. MONITORING AGENCY NAME & ADDRESS (if different from Controlling Office)	15. SECURITY CLASS. (of this report): UNCLASSIFIED
	15a. DECLASSIFICATION/DOWNGRADING SCHEDULE

16. DISTRIBUTION STATEMENT (of this Report)

Approved for public release; distribution unlimited.

DDC RECEIVED SEP 28 1977 B

17. DISTRIBUTION STATEMENT (of the abstract entered in Block 20, if different from Report)

18. SUPPLEMENTARY NOTES

Sponsored by Defense Advanced Research Projects Agency (DoD)
ARPA Order No. 2895.

19. KEY WORDS (Continue on reverse side if necessary and identify by block number)

Gravity Gradient, Gradiometer, Error Model.

20. ABSTRACT (Continue on reverse side if necessary and identify by block number)

Models are developed which characterize moving-base gravity gradiometer errors at the current state of the technology. Recent data reported by the Bell Aerospace Company, the Charles Stark Draper Laboratory and the Hughes Aircraft Company are used to compute error model parameters for each gradiometer. These error models are appropriate for determining the impact

(over)

DD FORM 1 JAN 73 1473 EDITION OF 1 NOV 65 IS OBSOLETE

UNCLASSIFIED

SECURITY CLASSIFICATION OF THIS PAGE (When Data Entered)

TABLE OF CONTENTS

TABLE OF CONTENTS (Continued)

LIST OF FIGURES

LIST OF TABLES

1. INTRODUCTION

1.1 BACKGROUND

Instruments to measure the spatial gradient of the earth's gravity field from a moving platform have been under consideration for over 10 years (Ref. 1). In that time gravity gradiometer development has progressed to a technical maturity level where instruments suitable for operating in a moving-base environment may be only a few years away. The Bell Aerospace Division of Textron is currently planning moving-base tests for their gradiometer on a linear laboratory track (Ref. 2). The Charles Stark Draper Laboratory is in the process of building a complete three-axis gradiometric triad with compensation for the jitter motion induced by platform stabilization control loops (Ref. 3). Hughes Aircraft Company is establishing moving-base platform requirements for their gradiometer (Ref. 4). In addition to these efforts the Navy Strategic Systems Project Office is sponsoring a gradiometer feasibility demonstration which is expected to lead to an advanced development gradiometer model suitable for at-sea testing in late 1981 (Ref. 5).

This report provides preliminary moving-base gradiometer error models appropriate for the analysis and design of survey/navigation systems employing gradiometers. The models herein are also intended to be used in algorithms for the optimal estimation of gravimetric quantities from gradiometer measurements. For example, when planning an airborne gradiometric survey, such as conceptualized in Fig. 1.1-1, key

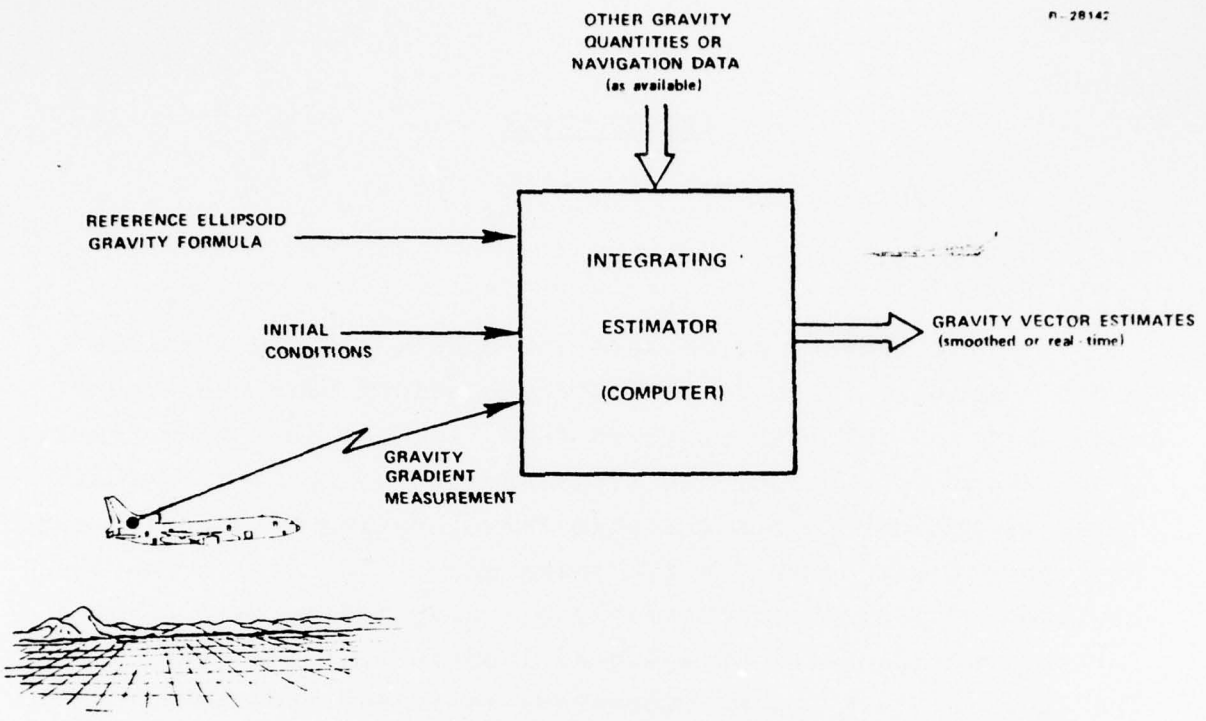

Figure 1.1-1 Moving-Base Gradiometric Recovery of the Gravity Vector

mission parameters such as track spacing, aircraft speed and altitude may be determined by analyses which have as inputs the gradiometer error models of this report. (Other inputs are statistical characterizations of the gravity field and accuracy models for other gravimetric sensors.)

When the survey is actually conducted, the same gradiometer error models are used again for the data processing. The models, when used in conjunction with optimal estimation algorithms and data from other gravimetric sensors, provide a basis for weighting the gradiometer measurements. Note that the optimal weight for gradiometer measurements vis-a-vis other gravimetric data are different at each gravity field wavelength. Gradiometers will provide the greatest quality of information in the short wavelength portion of the gravity field spectrum.

1.2 PURPOSE OF THIS REPORT

In order to adequately understand the advantages and limitations of gradiometers in relation to other gravimetric sensors, some characterization (i.e., a model) of gradiometer sensor errors is required. In past analyses white noise, first-order Markov or bias gradiometer models have been assumed (~~Refs. 6 through 9~~). Such models have been useful for providing insight into navigation, weapon system and gravity survey performance as a function of broad classes of gradiometer errors. In this role the generalized parametric models have provided indications of the benefits and limitations of gravity gradiometers. Now, as attention turns toward the application of specific gradiometer instruments (e.g., Bell, C[illegible] and Hughes) to particular survey and navigation missions, there is a need to assess the efficacy of different gravimetric sensors across all gravity field wavelengths which requires more than parametric representations of the effects of gradiometer error sources. The purpose of this report is to develop preliminary error models for each of the three gradiometers consistent with the current state of their technology. The utility of refined error models extends to other gradiometer applications as well. The models presented in this report are also suitable for studies of gradiometer-aided inertial navigation systems, gradiometric map matching and real-time gravity vector recovery using gradiometers. Another use envisioned for the models herein is the direct linking of gradiometer errors to the performance of particularly critical missions (e.g., launch area mapping). Such links offer an avenue of application-oriented feedback to the manufacturers by spotlighting the most serious gradiometer error sources.

1.3 PERSPECTIVE

Error model development for instruments whose design is still incomplete creates a trade-off between specificity and update frequency (greater model detail requires more frequent model changes as the gradiometer designs evolve). For this reason, error model formulations have been chosen for simplicity while preserving essential error elements and reflect only such basic considerations as sensor orientation with respect to vertical and output noise correlation. Thus as instruments are improved and more detailed data becomes available, updating the models should be a straightforward procedure. The extrapolation of laboratory data to possible future performance in the field is another area requiring careful attention. In this report it is assumed that results demonstrated in the laboratory will be capable of replication by operational moving-base gradiometers. This somewhat optimistic view is offset by restricting consideration only to demonstrated laboratory data; i.e., no allowance is made for the improvements expected by the manufacturers in the course of further development work.

It is also appropriate to distinguish the analysis error models of this report from the dynamic error models developed by the manufacturers and others (Refs. 10 through 12) primarily for purposes of instrument balance and compensation. While important to ongoing development, such detailed models are too specific at present for gradiometer system application analysis. The rationale for selecting an appropriate middle ground between simplicity and fine detail is presented in the previous paragraph. Of course when a gradiometer-carrying platform becomes well-defined and the effects of environmental factors such as angular and linear vibration, temperature, magnetic fiels, etc. are known, future

extensions of such detailed models may be useful for gradiometric performance projections at the system and multisystem level.

In Chapters 2 through 4, error models for each of the three gradiometer prototypes are presented. Chapter 5 presents summary observations and concluding recommendations.

2. ERROR MODEL FOR THE BELL ROTATING ACCELEROMETER GRAVITY GRADIOMETER

2.1 BRIEF REVIEW OF THE BELL GRADIOMETER

The Bell gradiometer (Fig. 2.1-1) uses four matched accelerometers mounted on a slowly rotating (0.25 Hz) table. The summed output of a pair of accelerometers on opposite sides of the table provides the fundamental gradient measurement. Two such accelerometer pairs, oriented at right angles, permit signal processing* which greatly reduces sensitivity to angular acceleration. Although the noise level of a "good" accelerometer near the 0.25 Hz rotation frequency is several orders of magnitude too large for the rotating accelerometer gradiometer application, Bell has extensively reworked their Model VII accelerometer to reduce thermal and electronic noise.

In addition to accelerometer modification they have incorporated continuous-time feedback balance loops to stabilize scale factors of the four accelerometers. Other feedback networks which compensate various order nonlinear responses of the accelerometers are also implementd. The outputs of the accelerometers are mixed, preamplified, band limited and demodulated at twice rotation frequency, the carrier frequency for the gravity gradient information. As a result of this processing two gradient measurements are produced, one at 0 deg phase and the other at 90 deg. One measurement consists of the difference between the two inline

*The processing consists of subtracting the summed output of each accelerometer pair.

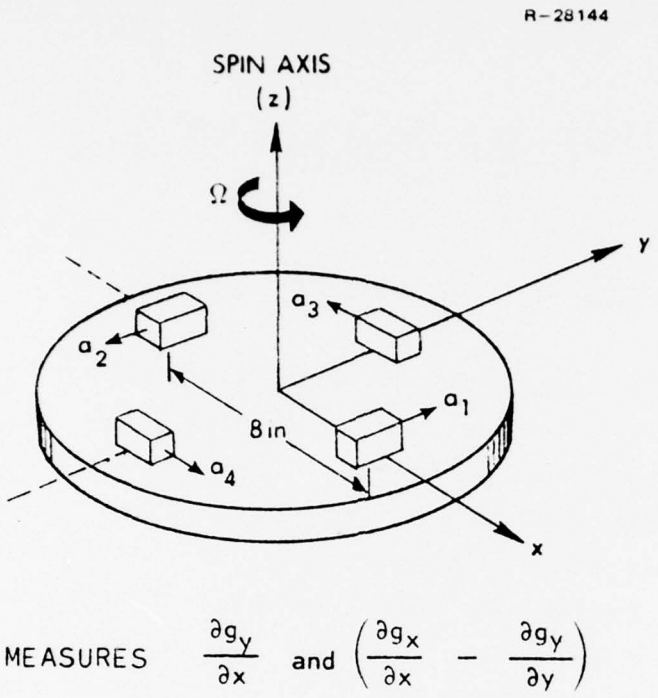

Figure 2.1-1 Idealization of the Bell Gradiometer

gradients lying in the plane of rotation. The second measurement is the rotation plane cross gradient. Because of the 90 deg phase difference between the two signals, inline gradients are demodulated in phase with the spatial axis reference (sine domodulator) and cross gradients are demodulated in quadrature (cosine demodulator). Since the gravity gradient signal is band-centered at twice the rotation frequency, the only error sources affecting the output are those with frequency components at or near 0.5 Hz (twice per revolution).

2.2 SUMMARY OF CURRENT BELL GRADIOMETER ERROR DATA

In Ref. 2, recent performance of the Bell gradiometer was summarized in the following areas:

- Zero offset and drift
- Output noise
- Noise power spectrum between 10^{-4} rad/sec and 10^{-1} rad/sec

Each category is now discussed.

2.2.1 Output Offset and Drift

Data given in Ref. 2 only apply to the case in which the gradiometer is oriented with the spin axis vertical. In this orientation DC outputs of the order of 50 EU* are reported. Recent conversations with Bell personnel indicate that zero offsets measured with the gradiometer spin axis horizontal are under 1500 EU. In Ref. 2 offset trends of 0.1 EU/hr are observed on both the sine and cosine channels with the spin axis vertical. Trend data with the spin axis horizontal are reported at 0.4 EU/hr for cross gradients and at 0.6 EU/hr for inline difference gradients.

2.2.2 Output Noise

Randomness figures for the Bell gradiometer have been computed by averaging data through a 10 second, double lag-filter† (two cascaded 10 second, first-order lags). The Bell data shows performance in all channels on the order of 1.8 EU rms. Although these data could be used as the basis for a white noise error model for the Bell gradiometer, the availability of error power spectra data permits more detailed modeling.

---

*One EU = 10^{-9} sec^{-2}.

†For white noise inputs, a 10 sec double lag filter is equivalent to a 40 sec moving window averager.

2.2.3 Noise Power Spectrum

The power spectrum of the Bell gradiometer noise is shown by the solid lines in Figs. 2.3-1. The data presented in the figures are taken from pages 33 and 35 of Ref. 2. In the following section an error model which consists of white noise driving third-order filters is used to characterize these data.

2.3 ERROR EQUATIONS

All error quantities described in this section apply to gradiometer instrument outputs, namely measurements of cross gradients and differenced pairs of inline gradients. A transformation which relates these quantities to elements of the gravity gradient tensor in an orthogonal, local-level coordinate frame is presented in Appendix A.

2.3.1 Output Offset and Drift

Offset and drift magnitude measurements for the Bell gradiometer are summarized in Table 2.3-1. A gradiometer triad with the three spin axes orthogonally oriented in the x, y and z directions defines the coordinate convention. The z-axis coincides with the local vertical.

The model for the zero offset of gradiometer measurements is a random constant given by the state equation set

$$\delta\dot{\underline{z}}_o = 0 \qquad (2.3\text{-}1)$$

where the elements of $\delta\underline{z}_o$ are arranged in the same order as in Table 2.3-1. The error covariance, P_{zo}, is defined as

R-28141

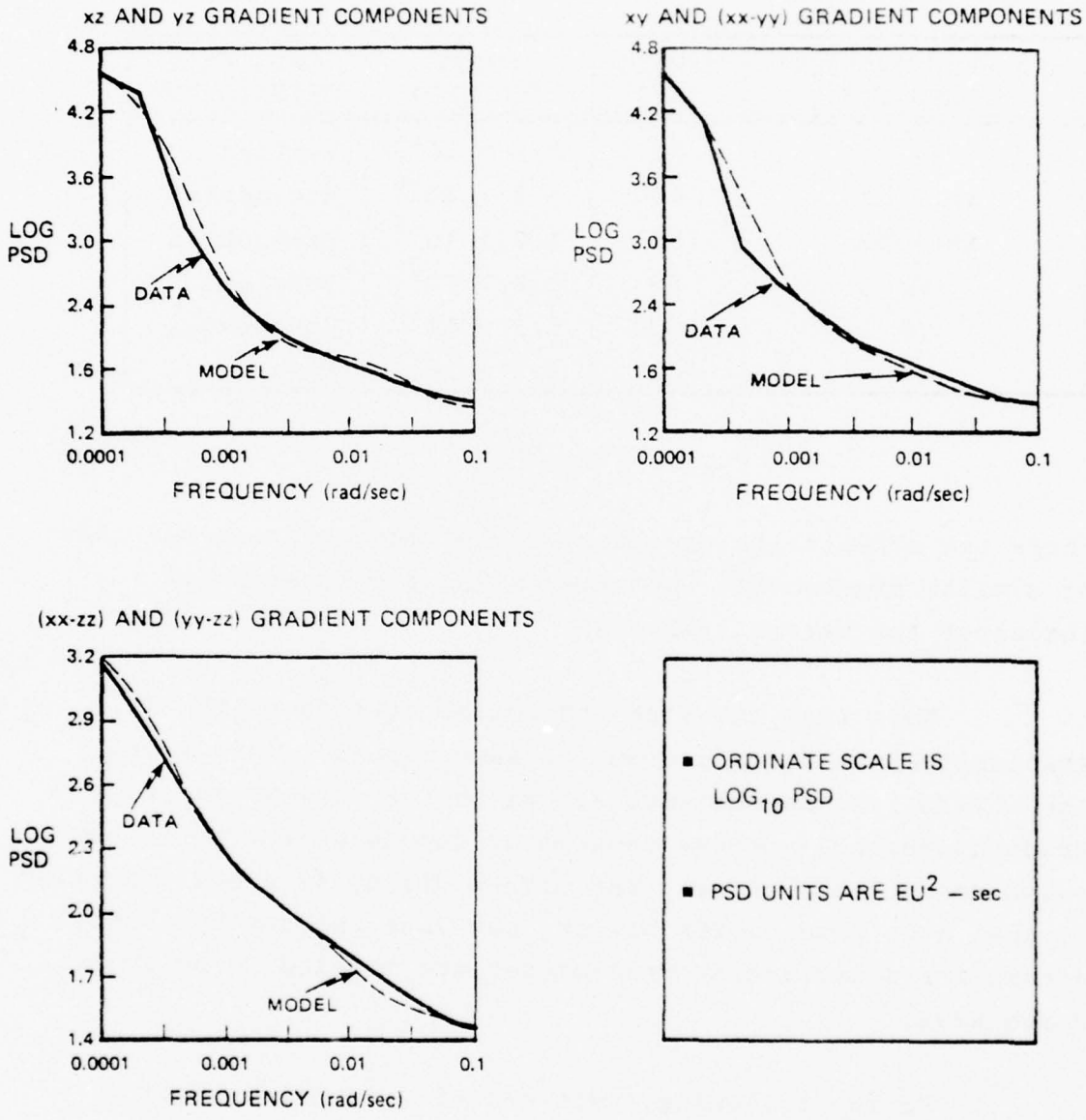

Figure 2.3-1 Error Power Spectra for the Bell Gradiometer

TABLE 2.3-1

OFFSET AND DRIFT DATA FOR THE BELL GRADIOMETER

MEASURED GRADIENT COMPONENT	OFFSET (EU)	DRIFT (EU/SEC)	SPIN AXIS ORIENTATION
xx - yy	50	2.8×10^{-5}	Vertical
yy - zz	1500	1.7×10^{-4}	Horizontal
xx - zz	1500	1.7×10^{-4}	Horizontal
xy	50	2.8×10^{-5}	Vertical
yz	1500	1.1×10^{-4}	Horizontal
xz	1500	1.1×10^{-4}	Horizontal

$$P_{zo} = E\left[\delta \underline{z}_o \; \delta \underline{z}_o^T\right] \qquad (2.3\text{-}2)$$

where the expectation operator, E, is taken over an ensemble of similar gradiometer instruments and the superscript $(\;)^T$ indicates the matrix transpose.

Note that the sine and cosine outputs of the Bell gradiometer are derived from the same signal. As a result, the only difference between errors on the inline and cross gradient channels occurs because of demodulator errors. Because demodulator offset (and offset drift) is a small portion of the total gradiometer offset, the sine and cosine channel errors for a particular gradiometer are modeled to be fully correlated.

In the following, zero offset (and offset drift) errors in different gradiometers of a triad are modeled as independent. Of course, future triad-level testing will identify platform-related error sources which will drive all three gradiometers. As such error sources are identified, the appropriate cross-covariance error terms can be updated accordingly. Using the data in the first column of Table 2.3-1, the offset error covariance P_{zo}, is

$$P_{zo} = \begin{bmatrix} 0.25 & 0 & 0 & 0.25 & 0 & 0 \\ 0 & 230 & 0 & 0 & 230 & 0 \\ 0 & 0 & 230 & 0 & 0 & 230 \\ 0.25 & 0 & 0 & 0.25 & 0 & 0 \\ 0 & 230 & 0 & 0 & 230 & 0 \\ 0 & 0 & 230 & 0 & 0 & 230 \end{bmatrix} \times 10^4 \text{ EU}^2 \qquad (2.3\text{-}3)$$

Because the data in Ref. 2 do not indicate the sign of zero offsets, both channels of a gradiometer are assumed to have the same sign. As a result all of the cross covariances in Eq. 2.3-3 are positive. Appropriate sign changes to these cross terms can be made when signed zero offset data is available for the Bell gradiometer.

The model for offset drift is given by the state equation set

$$\delta\dot{\underline{z}}_d = \underline{d} \qquad (2.3\text{-}4)$$

where $\underline{d}$ is the vector of drift coefficients. Drift is modeled in the same fashion as zero offset. The covariance, P_{zd}, of $\underline{d}$, defined as in Eq. 2.3.2, is computed from the second column of numbers in Table 2.3-1.

$$P_{zd} = \begin{bmatrix} 7.8 & 0 & 0 & 7.8 & 0 & 0 \\ 0 & 290 & 0 & 0 & 190 & 0 \\ 0 & 0 & 290 & 0 & 0 & 190 \\ 7.8 & 0 & 0 & 7.8 & 0 & 0 \\ 0 & 190 & 0 & 0 & 120 & 0 \\ 0 & 0 & 190 & 0 & 0 & 120 \end{bmatrix} \times 10^{-10} \text{EU}^2/\text{sec}^2 \qquad (2.3\text{-}5)$$

2.3.2 Output Noise

Noise power spectra for various outputs of the Bell gradiometer are presented as solid lines in Fig. 2.3-1. The power spectral density $S(\omega)$, plotted in Fig. 2.3-1, and its transform, the autocorrelation function $R(\tau)$, are related by

$$S(\omega) = \frac{1}{\pi} \int_{-\infty}^{\infty} R(\tau)\, e^{-j\omega\tau}\, d\tau \qquad (2.3\text{-}6a)$$

$$R(\tau) = \int_{0}^{\infty} S(\omega)\, e^{j\omega\tau}\, d\omega \qquad (2.3\text{-}6b)$$

where ω is the angular frequency in radians/sec and τ is the shift of the autocorrelation. Note that according to the definitions of Eqs. 2.3-6 the total power, $R(0)$ (i.e., the variance), is the unscaled area under $S(\omega)$ for positive frequency.

Rational functions of the form

$$F(\omega) = \frac{K^2(\omega^2+\beta_1^2)(\omega^2+\beta_2^2)(\omega^2+\beta_3^2)}{(\omega^2+\beta_4^2)(\omega^2+\beta_5^2)(\omega^2+\beta_6^2)} \qquad (2.3\text{-}7)$$

have been fitted to the gradiometer error spectra data of Fig. 2.3-1. Plots of the resulting analytic spectral densities are shown by the dashed lines in that figure. Note that Eq. 2.3-7 may be modeled by a white noise driven process in which the white noise of spectral density, Q, is given by

$$Q = \frac{K^2\ \beta_1^2\ \beta_2^2\ \beta_3^2}{\beta_4^2\ \beta_5^2\ \beta_6^2} \qquad (2.3\text{-}8)$$

and the transfer function it drives is

$$H_o(j\omega) = \frac{\beta_4\ \beta_5\ \beta_6(\beta_1+j\omega)(\beta_2+j\omega)(\beta_3+j\omega)}{\beta_1\ \beta_2\ \beta_3(\beta_4+j\omega)(\beta_5+j\omega)(\beta_6+j\omega)} \qquad (2.3\text{-}9)$$

The process noise corrupting each gradiometer measurement is modeled as uncorrelated across output channels of different gradiometers. However, as indicated in the discussion following Eq. 2.3-2 it is necessary to model the noise on both outputs of the same gradiometer as fully correlated.

Since spectral data for the Bell gradiometer are not available at frequencies higher than 0.1 rad/sec, some form of band limiting is appropriate. In view of the intended uses of the error models herein, namely optimal least squares data processing, reduction and simulation, it is desirable that any high frequency attenuation which is incorporated solely to bound error model response be dominated by the optimal estimator's high frequency characteristics. For most gravimetric and navigation-related applications a high frequency cutoff for the model will suffice which is one decade higher than the highest break frequency in the transfer function, $H_o(j\omega)$.

A form of band limiting particularly suited to both analysis in the time domain as well as the frequency domain is obtained by adding a third-order pole to $H_o(j\omega)$. With this addition, the transfer function for the final model is

$$H(j\omega) = \frac{\beta_7 H_o(j\omega)}{(\beta_7+j\omega)^3} \qquad (2.3\text{-}10)$$

The values of K and β_i (i=1,...,7) are summarized in Table 2.3-2. The complete model for a single Bell gradiometer instrument is presented in state space form in Fig. 2.3-2.

TABLE 2.3-2

SPECTRAL DENSITY ERROR MODEL PARAMETERS FOR THE BELL GRADIOMETER

MEASURED GRADIENT COMPONENT	K $(EU\text{-}SEC^{1/2})$	β_1 (SEC^{-1})	β_2 (SEC^{-1})	β_3 (SEC^{-1})	β_4 (SEC^{-1})	β_5 (SEC^{-1})	β_6 (SEC^{-1})	β_7 (SEC^{-1})	SPIN AXIS ORIENTATION
xx - yy	5.63	6.3×10^{-4}	2.8×10^{-3}	1.6×10^{-2}	1.8×10^{-4}	2.0×10^{-3}	10^{-2}	0.16	Ver.
yy - zz	5.27	6.3×10^{-4}	1.6×10^{-3}	1.8×10^{-2}	2.1×10^{-4}	2.1×10^{-4}	10^{-2}	0.18	Hor.
xx - zz	5.27	6.3×10^{-4}	1.6×10^{-3}	1.8×10^{-2}	2.1×10^{-4}	2.1×10^{-4}	10^{-2}	0.18	Hor.
xy	5.63	6.3×10^{-4}	2.8×10^{-3}	1.6×10^{-2}	1.8×10^{-4}	2.0×10^{-3}	10^{-2}	0.16	Ver.
yz	4.54	10^{-3}	1.6×10^{-3}	5.0×10^{-2}	2.6×10^{-4}	2.6×10^{-4}	2.5×10^{-2}	0.5	Hor.
xz	4.54	10^{-3}	1.6×10^{-3}	5.0×10^{-2}	2.6×10^{-4}	2.6×10^{-4}	2.5×10^{-2}	0.5	Hor.

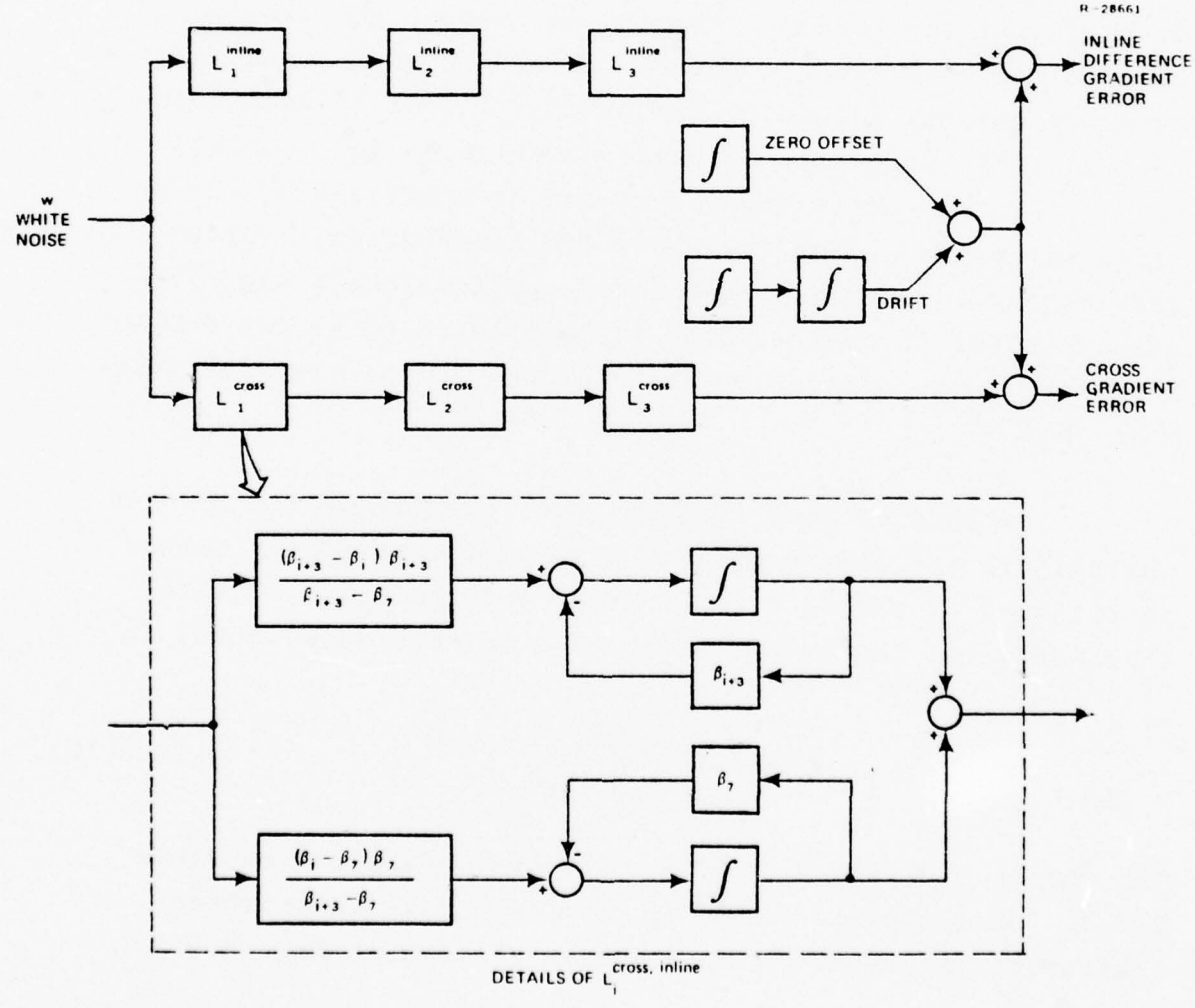

Figure 2.3-2 Bell Gradiometer Error Model (Per Axis)

The models presented in this section apply to the outputs of the Bell gradiometer. Since these measurements do not necessarily correspond to elements of the gravity gradient tensor, certain transformations are required to convert the error models herein to "tensor level" error models. More detailed discussion is presented in Appendices A and B.

Before concluding this section, it is worthwhile to dwell briefly on the transform definitions of Eqs. 2.3-6. Often in analytical work the alternative "two-sided" transform pair

$$S_1(\omega) = \int_{-\infty}^{\infty} R(\tau)\, e^{-j\omega\tau}\, d\tau \qquad (2.3\text{-}11a)$$

$$R(\tau) = \frac{1}{2\pi} \int_{-\infty}^{\infty} S_1(\omega)\, e^{j\omega\tau}\, d\omega \qquad (2.3\text{-}11b)$$

is employed. In an analysis system based on Eqs. 2.3-11 note that the spectral density, S_1, is defined such that

$$S_1(\omega) = \pi\, S(\omega) \qquad (2.3\text{-}12)$$

The spectral model given by Eqs. 2.3-7 through 2.3-10 uses Eqs. 2.3-6 to define the transform pair.

3. ERROR MODEL FOR THE CSDL* FLOATED GRAVITY GRADIOMETER

3.1 BRIEF REVIEW OF THE CSDL GRADIOMETER

The CSDL gradiometer (Fig. 3.1-1) employs a floated, electrostatically-suspended sphere with dense material packed symmetrically about opposite poles of the sphere. Gravity gradients induce a torque on the sphere that is sensed through the electrical currents needed to hold the sphere in its nominal attitude. The sensor is not rotated; hence parameters affecting the low frequency and DC performance of the sensor are critical and must be held to close tolerances. The final balancing of the float is controlled by an internal electrostatic discharge (sputtering) system which transports small amounts of gold across electrode gaps inside the sphere.

The floatation chamber interior is temperature stabilized to one microdegree Fahrenheit to achieve neutral buoyancy and prevent thermally induced shear motion of the fluid. CSDL personnel also believe that a very high degree of floatation fluid (Freon†) purity may be required as well to prevent fluid shears. Impurity-induced shears may result from the gravity-induced pressure field causing settling of different density components of the fluid.

Other significant error sources affecting the CSDL gradiometer are the thermal noise limit associated with

---

*Charles Stark Draper Laboratory.

†Trademarked product of E.I. duPont de Nemours Co.

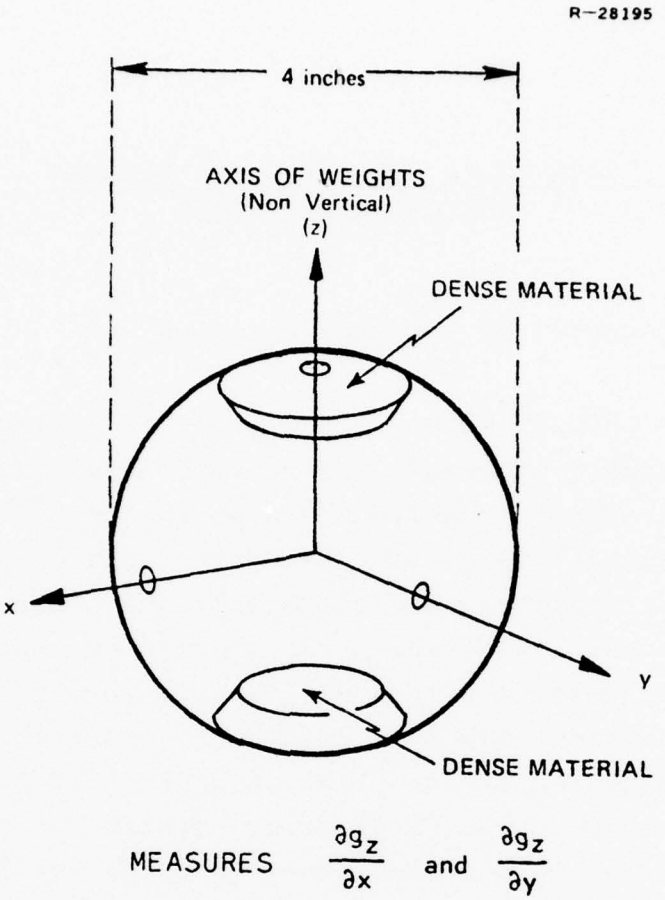

Figure 3.1-1 CSDL Gradiometer Float Element

Brownian motion of the floatation fluid molecules and small changes in the mass balance of the sensor. These small mass variations, believed due to minute deformations or "creep" of the float by the fluid pressure field, manifest themselves as changes in the long-period (many days) drift rate of the gradiometer.

3.2 SUMMARY OF CURRENT FLOATED GRAVITY GRADIOMETER ERROR DATA

In Ref. 3, data is provided on zero offset, drift and output noise. Because the axis of weights of the floated gradiometer is aligned at an angle of 35.2644 deg with the vertical, the data reported by CSDL is a superposition of

"vertical" and "horizontal" gravity gradients. The reduction of the gradiometer measurements to elements of the gravity gradient tensor expressed in an orthogonal reference frame requires a suitable transformation (Appendix C). For this reason it is incorrect to view the data and models which follow as representing either "horizontal" or "vertical" gradient errors.

3.2.1 Output Offset and Drift

Zero offset and offset drift data for the cross gradients $\partial g_z/\partial x$ and $\partial g_z/\partial y$* are summarized in Table 3.2-1. The data comes from Ref. 3 (pages 47 through 101).**

TABLE 3.2-1
OFFSET AND DRIFT DATA FOR CSDL GRADIOMETER

CSDL TEST NUMBER	ZERO OFFSET (EU)		DRIFT (EU/HR)	
	$\partial g_z/\partial x$ †	$\partial g_z/\partial y$ ‡	$\partial g_z/\partial x$ †	$\partial g_z/\partial y$ ‡
0035	-224.7	997.7	2.199	0.983
0042	351.2	-757.2	1.012	0.379
0050	652.9	-647.3	0.480	0.212
0054	727.3	-617.4	0.168	0.126
0055	752.7	-595.6	-0.075	0.139
rss of above data	582.2	738.2	1.11	0.488

† Corresponds to CSDL M_L torque measurements

‡ Corresponds to CSDL M_Z torque measurements

*The float body coordinate frame for these measurements is presented in Fig. 3.1-1.

**As updated by CSDL.

3.2.2 Output Noise

Two forms of noise data are available for the CSDL gradiometer. In Ref. 3 both fifteen minute averages of gradiometer output and twenty minute noise records are presented. The gradiometer dynamics and filtering associated with the 20 minute noise data as given in Ref. 3 are reproduced in Fig. 3.2-1. The noise output of the filter is 0.36 EU rms for $\partial g_z/\partial x$ and 0.49 EU rms for $\partial g_z/\partial y$.

3.3 ERROR EQUATIONS

To account for the different set of body axis coordinates for each sensor* of a gradiometer triad subscripts one through three are used to identify the measurements provided by the individual gradiometers. Hence the full measurement set provided by the sensor triad is

$$\underline{z} = \begin{bmatrix} \frac{\partial g_{z1}}{\partial x_1} \\ \frac{\partial g_{z1}}{\partial y_1} \\ \frac{\partial g_{z2}}{\partial x_2} \\ \frac{\partial g_{z2}}{\partial y_2} \\ \frac{\partial g_{z3}}{\partial x_3} \\ \frac{\partial g_{z3}}{\partial y_3} \end{bmatrix} + \delta\underline{z}(\text{errors}) \qquad (3.3\text{-}1)$$

*To recover all of the elements of the gravity gradient tensor the axes of weights of CSDL sensor triad must be skew aligned.

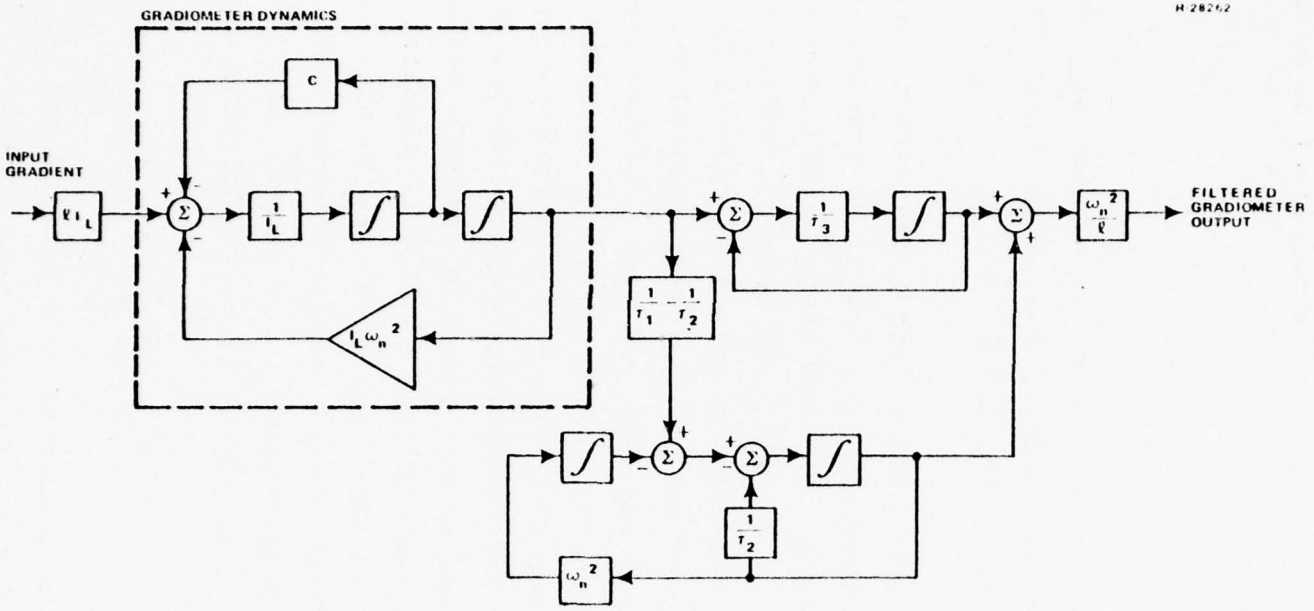

Figure 3.2-1 Signal Block Diagram of CSDL Gradiometer and Filter

3.3.1 Output Offset and Drift

The error model for zero offset is a vector of random constants

$$\delta\dot{\underline{z}}_o = 0 \qquad (3.3\text{-}2)$$

where the elements of the error vector, $\delta\underline{z}_o$, are arranged in the same order as in Eq. 3.3-1. The offset error covariance, P_{zo}, is defined by Eq. 2.3-2.

The zero offset (and offset drift) errors in different CSDL gradiometers of a triad are modeled as independent random constants. The rationale is the same as for rotating gradiometers (i.e., Bell and Hughes), namely that the chief cause of any correlation between errors in different gradiometer instruments will be platform-related sources. Such sources are not yet well defined. However significant correlation is expected between errors in the two cross gradient outputs of each CSDL sensor. This correlation should not be as strong as the correlation between errors of a single Bell or Hughes gradiometer since the two CSDL sensor outputs are derived from two distinct electrical signals. The electrical signals, in turn, are generated to null torques about orthogonal float element axes. To model this correlation the sample covariance, $\tilde{p}_{ij}$, of the i^{th} and j^{th} output measurements (i=1,2, j=1,2) is computed using the equation

$$\tilde{p}_{ij} = \frac{1}{n}\sum_{k=1}^{n} \delta z_{ik}\,\delta z_{jk} \qquad (3.3\text{-}3)$$

where n is the number of data samples and z_{ik} is the k^{th} zero offset (or drift) error measurement of the i^{th} gradiometer output channel. Equation 3.3-3 provides an unbiased, maximum likelihood estimate of p_{ij} for independent measurements of normally distributed zero offsets (or offset drifts).

Using Eq. 3.3-3 and the data in Table 3.2-1, the output offset error covariance is

$$P_{zo} = \begin{bmatrix} 3.39 & -3.62 & 0 & 0 & 0 & 0 \\ -3.62 & 5.45 & 0 & 0 & 0 & 0 \\ 0 & 0 & 3.39 & -3.62 & 0 & 0 \\ 0 & 0 & -3.62 & 5.45 & 0 & 0 \\ 0 & 0 & 0 & 0 & 3.39 & -3.62 \\ 0 & 0 & 0 & 0 & -3.62 & 5.45 \end{bmatrix} \times 10^5 \text{ EU}^2 \tag{3.3-4}$$

The error model for drift is

$$\delta \dot{\underline{z}}_d = \underline{d} \tag{3.3-5}$$

where the elements of $\underline{d}$ are the drift coefficients ordered in the same fashion as in Eq. 3.3-1. The covariance, P_{zd}, of $\underline{d}$, defined as in Eq. 2.3-2 is computed from Table 3.2-1 and Eq. 3.3-3 in the same manner as the offset error covariance.

$$P_{zd} = \begin{bmatrix} 9.45 & 4.10 & 0 & 0 & 0 & 0 \\ 4.10 & 1.84 & 0 & 0 & 0 & 0 \\ 0 & 0 & 9.45 & 4.10 & 0 & 0 \\ 0 & 0 & 4.10 & 1.84 & 0 & 0 \\ 0 & 0 & 0 & 0 & 9.45 & 4.10 \\ 0 & 0 & 0 & 0 & 4.10 & 1.84 \end{bmatrix} \times 10^{-8} \text{ EU}^2/\text{sec}^2 \tag{3.3-6}$$

Note that the very high correlation between the offset and drift errors of the gradiometer's two outputs tend to confirm the CSDL contention that these error sources originate in the sensor, rather than in the electronic processing and control systems.

3.3.2 Output Noise

The output noise of the CSDL gradiometer is appropriately modeled by white noise driving the filter depicted in Fig. 3.2-1. The model for each pair of sensor outputs is illustrated in Fig. 3.3-1.

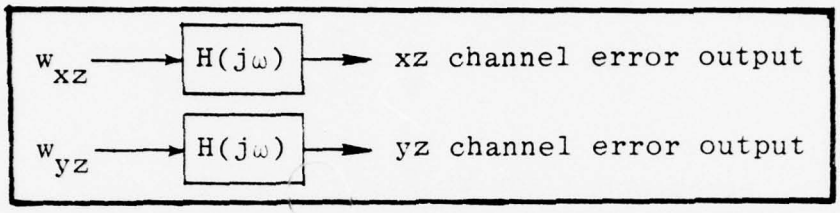

Figure 3.3-1 Noise Error Model for CSDL Gradiometer Sensor

In Fig. 3.3-1 the transfer function $H(j\omega)$ represents the gradiometer dynamics and filter shown in Fig. 3.2-1. The quantities w_{xz} and w_{yz} are white noise errors referred to the inputs of the $\partial g_z/\partial x$ and $\partial g_z/\partial y$ channels respectively. Note that, in terms of Fig. 3.2-1, the transfer function $H(j\omega)$ for an ideal gradiometer (noise-free) is

$$H(j\omega) = \frac{\text{Filtered Gradiometer Output}}{\text{Value of the Gravity Gradient}} \qquad (3.3\text{-}7)$$

The filter parameters currently used by CSDL are

$I_L = 11{,}717 \text{ gm-cm}^2$

$C = 1080 \text{ dyn-cm-sec}$

$\omega_n = 0.1066 \text{ sec}^{-1}$

$\tau_1 = 11 \text{ sec}$

$\tau_2 = 4.47 \text{ sec}$

$\tau_3 = 5.78 \text{ sec}$

$\ell = 0.65$

The inertia efficiency of the float, ℓ, is given here for reference purposes only as it cancels out of $H(j\omega)$. With the parameters given on the previous page the gradiometer and filter transfer function corresponding to Fig. 3.2-1 is:

$$H(j\omega) = \frac{4.569 \times 10^{-4}(j\omega)^2 + 0.091(j\omega) + 0.01136}{\left[(j\omega)+0.173\right]\left[(j\omega)^2+0.2237(j\omega)+0.01136\right]\left[(j\omega)^2+0.08535(j\omega)+0.01136\right]} \qquad (3.3\text{-}8)$$

Using the transform pair definition of Eqs. 2.3-11 the relation between the spectral density, Q, of white noise driving $H(j\omega)$ and the variance, σ^2, of the output is found to be

$$Q = 53.1\ \sigma^2 \qquad (3.3\text{-}9)$$

From Eq. 3.3-9 and the rms noise values given in Section 3.2 the white noise spectral densities for the model are

$$Q_{xz}(\text{spectral density of } w_{xz}) = 6.88\ EU^2\text{-sec} \qquad (3.3\text{-}10a)$$

$$Q_{yz}\ (\text{spectral density of } w_{yz}) = 12.75\ EU^2\text{-sec} \qquad (3.3\text{-}10b)$$

Current CSDL data is in a format which makes the determination of cross correlation between w_{xz} and w_{yz} difficult. It is anticipated that the model will be updated to include such cross correlation as suitable data becomes available.

4. ERROR MODEL FOR THE HUGHES ROTATING GRAVITY GRADIOMETER (RGG)

4.1 BRIEF REVIEW OF THE HUGHES GRADIOMETER

The Hughes gradiometer (Fig. 4.1-1) employs two sets of sensor arms with dense masses at the ends which are torqued by the earth's gravity gradient field. The sensor arms are maintained at right angles to each other by torsion pivots which link the arm centers and the case. This assembly is rotated at a frequency* such that the differential mode† of arm-pivot system is excited by the gravity gradient torque. The high Q‡ associated with the system provides mechanical resonant amplification of the differential mode gradient signal by approximately 40 dB. In addition the rotation separates, in frequency, gravity gradient signals and much of the accompanying measurement noise. The differential mode motion is sensed by a piezoelectric transducer, amplified, filtered, frequency modulated and transmitted from the rotating assembly to electronics mounted on the case of the gradiometer.

In the RGG, as in the Bell gradiometer, the signal is demodulated at twice rotation frequency into sine and cosine channels to provide two gradient measurements - the cross gradient defined by the plane of rotation of the

---

*The rotation frequency most recently used by Hughes is 17.55 Hz (RGG #2).

†i.e., the mode in which the sensor arms are deflected oppositely.

‡Q is energy stored divided by energy dissipated in one oscillatory cycle.

gradiometer and the difference between the two inline gradients corresponding to the plane of rotation (illustrated in Fig. 4.1-1). Coordinate axes of a suitable earth-fixed reference frame are selected by phase shifting the sine and cosine demodulators to the appropriate initial angular reference. Because the gravity gradient signal is encoded at a small bandwidth centered at twice the rotation frequency, the only error sources which propagate through the instrument are those at or near twice spin frequency. Note that, in this regard, the frequency characteristics of the Hughes instrument are similar to those of the Bell gradiometer.

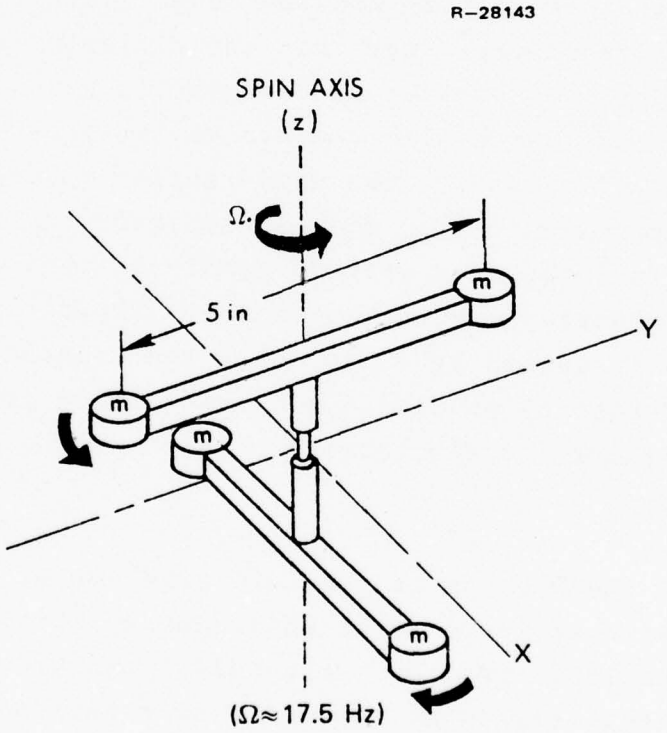

Figure 4.1-1 Idealization of Hughes Gradiometer

4.2 SUMMARY OF CURRENT GRADIOMETER ERROR DATA

In Ref. 4, current test data for the Hughes gradiometer are given for output offset and short term randomness. No long term drift data are available since neither of two operating Hughes gradiometers have been groomed for long term operation. Since the gradiometer instrument outputs must be transformed to express the individual gravity gradient tensor elements, Hughes has approximated the effects of the transformation by dividing their gradiometer measurements by two. In the sequel it will be more convenient to use the actual instrument outputs as a data reference.

4.2.1 Output Offset

The output magnitude of the gradiometer while operating in the laboratory has been measured to be as low as 52.5 EU (Ref. 13) with the spin axis vertical and 30.5K EU with the spin axis horizontal. Although these values will probably be reduced significantly in the near future, they represent the instrument's present performance. The trend of this offset data is not available from test results reported to date.

4.2.2 Output Noise

Random variation of the Hughes gradiometer output is reported as 2 EU rms for the vertical spin axis orientation and 25 EU rms for the horizontal spin axis orientation. Hughes indicates that these values correspond to a 20 sec* averaging time when referred to a white noise driven moving window averager approximately representing the gradiometer and signal processing dynamics. Of course, after demodulation, actual gradiometer errors are band limited rather than white. Nonetheless, in the absence of power spectral density data or long time-history records of gradiometer operation, white noise offers a convenient means for representing random errors in the Hughes instrument.

*Equivalent to a 10 sec first-order lag.

The noise model for the RGG treats the sine and cosine channel errors as fully correlated error sources. The model is similar to the Bell gradiometer error model in this regard. Further testing of the instrument will define the extent of actual correlation between output errors of the same RGG. It is anticipated that such data will be incorporated into the models as it becomes available.

4.3 ERROR EQUATIONS

The data given in Section 4.2 has been scaled by the factor 1/2. It is convenient to rescale by that factor so that the data corresponds to the measured gradiometer outputs. In the tabulations which follow the distinction between data provided by Hughes and the corresponding re-scaled data is clearly delineated.

4.3.1 Output Offset

RGG offset measurements are summarized in Table 4.3-1.

TABLE 4.3-1
RGG OUTPUT OFFSET DATA

T-1154

MEASURED GRADIENT COMPONENT	PROVIDED BY HUGHES - EU	REFERENCED TO GRADIOMETER OUTPUTS - EU	SPIN AXIS ORIENTATION
xx - yy	52.5	105	Vertical
yy - zz	30.5 K	71 K	Horizontal
xx - zz	30.5 K	71 K	Horizontal
xy	52.5	105	Vertical
yz	30.5K	71 K	Horizontal
xz	30.5K	71 K	Horizontal

The model for gradiometer offset is a random constant given by the state equation set

$$\delta\dot{\underline{z}}_o = 0 \qquad (4.3\text{-}1)$$

where the elements of $\delta\underline{z}_o$ are defined in the same fashion as $\delta\underline{z}$. The zero offset model has the same correlation structure as that of the Bell gradiometer, namely offsets in the sine and cosine channels are modeled to be fully correlated and offsets for different gradiometer instruments in the triad are modeled to be independent. The more detailed explanation in Section 2.3.1 also applies to the Hughes gradiometer. The covariance, P_{zo}, defined by Eq. 2.3-2, is computed from the second column of numbers in Table 4.3-1. The value of P_{zo} is

$$P_{zo} = \begin{bmatrix} 0.011 & 0 & 0 & 0.011 & 0 & 0 \\ 0 & 5.0\times10^3 & 0 & 0 & 5.0\times10^3 & 0 \\ 0 & 0 & 5.0\times10^3 & 0 & 0 & 5.0\times10^3 \\ 0.011 & 0 & 0 & 0.011 & 0 & 0 \\ 0 & 5.0\times10^3 & 0 & 0 & 5.0\times10^3 & 0 \\ 0 & 0 & 5.0\times10^3 & 0 & 0 & 5.0\times10^3 \end{bmatrix} \times 10^6 \text{ EU}^2 \qquad (4.3\text{-}2)$$

Only the unsigned offset magnitudes have been provided by Hughes. Thus all of the cross covariances in Eq. (4.3-2) are positive.*

4.3.2 Output Noise

The RGG noise measurements given in Section 4.2 are summarized in Table 4.3-2. The spectral density of white noise which models the RGG randomness error is given by the third column of numbers. Units of spectral density are defined by the transform pair of Eqs. 2.3-11. The noise which models errors on the sine and cosine channel of a single gradiometer is taken to be fully correlated (as discussed in the paragraph proceeding Eq. 4.3-2).

*The discussion in the paragraph following Eq. 2.3-3 also applies to Eq. 4.3-2.

TABLE 4.3-2

RGG RANDOMNESS DATA

T-1155

MEASURED GRADIENT COMPONENT	PROVIDED BY HUGHES - EU (20 SEC MWA)*	REFERENCED TO GRADIOMETER OUTPUTS - EU (20 SEC MWA)	WHITE NOISE SPECTRAL DENSITY (EU^2 - SEC)	SPIN AXIS ORIENTATION
xx - yy	2	4	320	Vertical
yy - zz	25	50	5×10^4	Horizontal
xx - zz	25	50	5×10^4	Horizontal
xy	2	4	320	Vertical
yz	25	50	5×10^4	Horizontal
xz	25	50	5×10^4	Horizontal

*Moving Window Average

Note that the error models provided in this section correspond to measured outputs of the RGG. Models for the effect of RGG errors at the gradient tensor element level are found from the models herein and application of equations presented in Appendices A and B.

5. CONCLUSIONS AND RECOMMENDATIONS

This report describes new, data-derived error models for the Bell, CSDL and Hughes gradiometers. The models are useful for evaluating the effects of gradiometer errors on multisensor gravimetric surveys which incorporate moving-base measurements of the earth's gravity gradient field. The mathematical structure of these error models has been chosen so they are also useful for optimally estimating gravimetric quantities from gradiometer data. The models are preliminary because gradiometer instrument development is still incomplete. Although only a very limited set of missions could gainfully employ gradiometer technology at its current level, it is aapropriate to note that progress in the development of moving-base instruments by all three manufacturers has been rapid. Advantage should be taken of these results by continuing current programs of development and analysis. Specific recommendations directed toward the ongoing gradiometer development effort include maintaining and updating the error models in this report, applying the models to processing laboratory gradiometer data and exercising a posture which assures that the gradiometer is developed as a broadly applicable, multi-mission instrument.

Finally, attention is drawn to a technical area which deserves investigation, namely optimal estimation of gravity gradient tensor elements* from gradiometer output measurements. In addition, the potential benefits associated with a nonorthogonal choice of gradiometer instrument axis directions (to maximize gradient information output from a

*Present gradiometer prototypes do not provide all of the gravity gradient tensor elements directly.

triad of the next generation of sensors) merit consideration. An analysis of gradiometer performance improvements associated with such design modifications should address the following important issues:

- What is the optimal alignment for the axes of each gradiometer in a triad based on current error models?
- How much is the error reduced at the gradient tensor level and in estimates of the gravity disturbance vector associated with optimal gradiometer axis alignment in the triad?
- What is the design cost and the impact of additional data reduction complexity associated with adopting an optimal triad alignment configuration?

The resolution of these issues will provide an assessment of the advantages and disadvantages of non-orthogonal gradiometric sensor triad designs.

APPENDIX A

LEAST SQUARES REDUCTION OF INLINE GRAVITY GRADIENT MEASUREMENTS

The Bell and the Hughes gradiometers do not measure the inline gradients γ_{xx}, γ_{yy} and γ_{zz} directly. Instead the quantities provided by a rotating gradiometer are

$$z_1 = \gamma_{xx} - \gamma_{yy} + v_1 \tag{A-1a}$$

$$z_2 = \gamma_{yy} - \gamma_{zz} + v_2 \tag{A-1b}$$

$$z_3 = \gamma_{xx} - \gamma_{zz} + v_3 \tag{A-1c}$$

where v_i is noise on the i^{th} measurement. With the use of Laplace's equation

$$\gamma_{xx} + \gamma_{yy} + \gamma_{zz} = 0 \tag{A-2}$$

the augmented measurement set is given by

$$\underline{z} = H\underline{x} + \underline{v} \tag{A-3}$$

where

$$\underline{z} = \begin{pmatrix} z_1 \\ z_2 \\ z_3 \\ 0 \end{pmatrix} \tag{A-4}$$

$$\underline{x} = \begin{pmatrix} \gamma_{xx} \\ \gamma_{yy} \\ \gamma_{zz} \end{pmatrix} \tag{A-5}$$

$$H = \begin{bmatrix} 1 & -1 & 0 \\ 0 & 1 & -1 \\ 1 & 0 & -1 \\ 1 & 1 & 1 \end{bmatrix} \tag{A-6}$$

$$\underline{v} = \begin{bmatrix} v_1 \\ v_2 \\ v_3 \end{bmatrix} \tag{A-7}$$

If $\underline{v}$ is independent of $\underline{x}$ the least squares estimate of $\underline{x}$ is given by

$$\hat{\underline{x}} = H^{\#}\underline{z} \tag{A-8}$$

where $H^{\#}$ is the optimal estimator (Ref. 14) given by

$$H^{\#} = (H^T R^{-1} H)^{-1} H^T R^{-1} \tag{A-9}$$

and R is the covariance of $\underline{v}$.

Note that if the elements of $\underline{v}$ are not independent, an appropriate "whitening" transformation must be applied to Eq. A-3 before computing $H^{\#}$. Because the order of the equation sets associated with gradiometer measurements seldom exceeds seven, computation of the necessary whitening transformation is not difficult. For the matrix H, as given by Eq. A-6 and the same noise variance in each channel, $H^{\#}$ has the value

$$H^{\#} = \frac{1}{3} \begin{bmatrix} 1 & 0 & 1 & 1 \\ -1 & 1 & 0 & 1 \\ 0 & -1 & -1 & 1 \end{bmatrix} \tag{A-10}$$

Since the fourth element of $\underline{z}$ is zero, the transformation between the gradiometer measurements and elements of the gradient tensor is effectively given by deleting the fourth column of $H^{\#}$. In this case the least squares estimate of the gradient tensor elements can be written

$$\begin{pmatrix} \hat{\Gamma}_{xx} \\ \hat{\Gamma}_{yy} \\ \hat{\Gamma}_{zz} \end{pmatrix} = \frac{1}{3} \begin{bmatrix} 1 & 0 & 1 \\ -1 & 1 & 0 \\ 0 & -1 & -1 \end{bmatrix} \begin{bmatrix} z_1 \\ z_2 \\ z_3 \end{bmatrix} \qquad \text{(A-11)}$$

Note that, in addition to introducing the scale factor of 1/3 between measured gradient data and the actual tensor elements, Eq. A-11 defines correlation between estimates of the inline gravity gradients. Equation A-3 substituted into Eq. A-11 shows that the same correlation structure also applies to the <u>error</u> in the estimated gradients.

APPENDIX B

TRANSFORMATION OF GRADIOMETER MEASUREMENT ERROR MODELS INTO TENSOR ELEMENT ERROR MODELS

The output equation for the Bell and Hughes gradiometer is of the form

$$y = (\gamma_{xx}-\gamma_{yy}) \sin 2\Omega t + 2\gamma_{xy} \cos 2\Omega t \qquad \text{(B-1)}$$

where Ω is the rotation rate and t is time. Because it is often the practice of the manufacturers to scale noise measurements to the sine and cosine terms of Eq. B-1 (i.e., sine channel and cosine channel output), transforming from gradiometer output to the gravity gradient tensor involves

- Applying Eq. A-10 to the inline difference terms
- Scaling the cross terms by 1/2.

Extending the notation of Appendix A to cross gradients indicated by mixed subscripts, the relation between a full triad of gradiometer measurements, $\underline{z}$, containing white noise errors of the same spectral density and estimates of the elements of the gravity gradient tensor, $\hat{\underline{\Gamma}}$, is

$$\hat{\underline{\Gamma}} = T\,\underline{z} \qquad \text{(B-2)}$$

where

$$\hat{\underline{\Gamma}} = \begin{bmatrix} \hat{\gamma}_{xx} \\ \hat{\gamma}_{yy} \\ \hat{\gamma}_{zz} \\ \hat{\gamma}_{xy} \\ \hat{\gamma}_{yz} \\ \hat{\gamma}_{xz} \end{bmatrix} \tag{B-3}$$

$$\underline{z} = \begin{bmatrix} z_1 \\ z_2 \\ z_3 \\ z_{xy} \\ z_{yz} \\ z_{xz} \end{bmatrix} \tag{B-4}$$

$$T = \begin{bmatrix} 1/3 & 0 & 1/3 & 0 & 0 & 0 \\ -1/3 & 1/3 & 0 & 0 & 0 & 0 \\ 0 & -1/3 & -1/3 & 0 & 0 & 0 \\ 0 & 0 & 0 & 1/2 & 0 & 0 \\ 0 & 0 & 0 & 0 & 1/2 & 0 \\ 0 & 0 & 0 & 0 & 0 & 1/2 \end{bmatrix} \tag{B-5}$$

The covariance relation corresponding to Eq. B-2 is

$$E\left[\underline{\Gamma}\ \underline{\Gamma}^T\right] = T\ E\left[\underline{z}\ \underline{z}^T\right]\ T^T \tag{B-6}$$

As an example, when Eqs. B-2 and B-6 are applied to the Hughes gradiometer, the tensor level randomness model depicted by Fig. B-1 is obtained. In Fig. B-1 the quantity v is white noise.

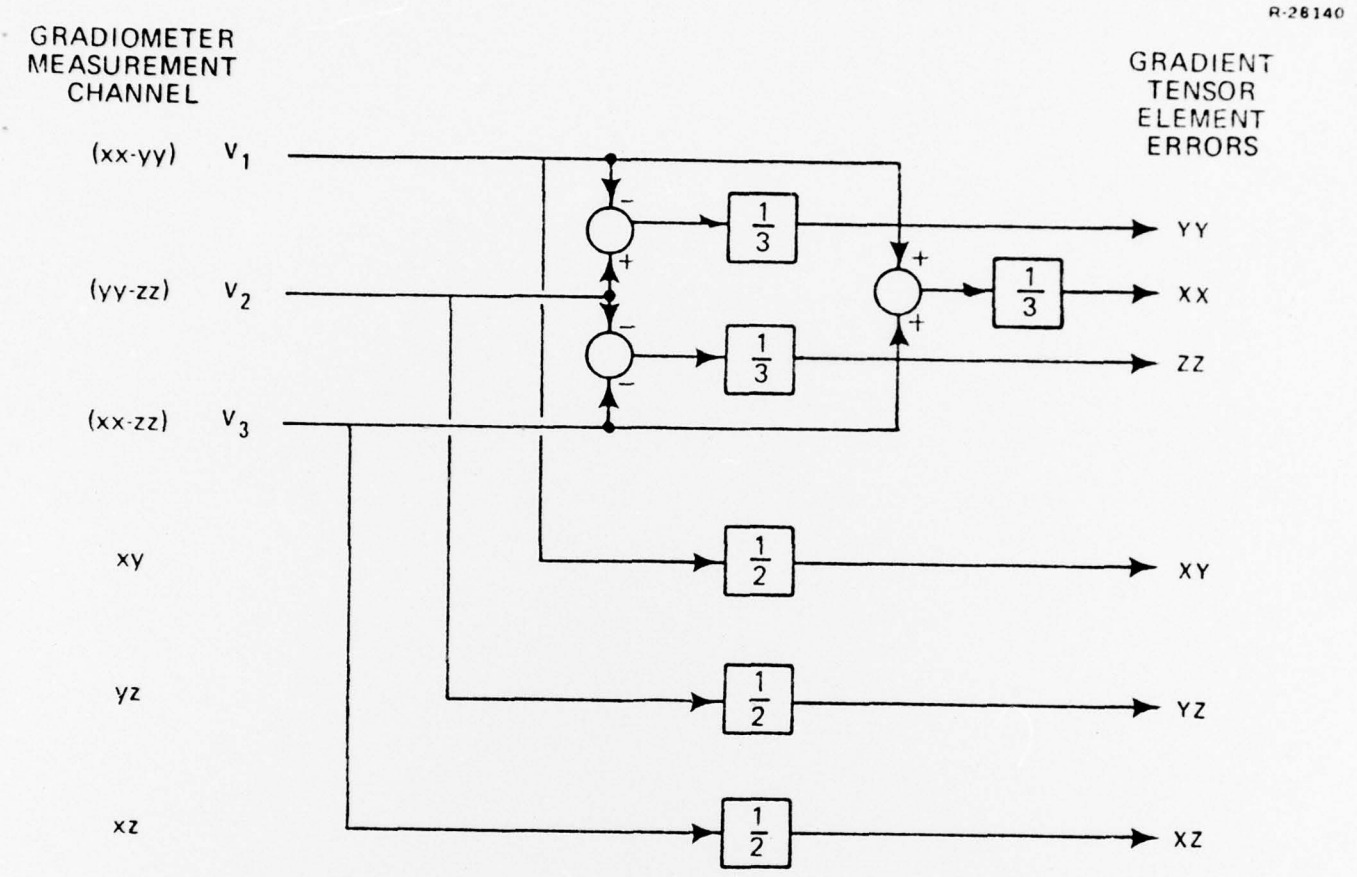

Figure B-1 Randomness Error Model for Hughes Gradiometer Triad

APPENDIX C

TRANSFORMATION BETWEEN CSDL GRADIOMETER MEASUREMENTS (AND MEASUREMENT ERRORS) AND ELEMENTS OF THE GRAVITY GRADIENT TENSOR EXPRESSED IN AN ORTHOGONAL REFERENCE FRAME

A complete CSDL gradiometer employs a nonorthogonal sensor triad as shown in Fig. C-1 to produce measurements which span the entire space of the earth's gravity gradient tensor. To reduce these measurements to elements of the gravity gradient tensor expressed in cluster-centered coordinates x', y', z', a set of linear relations between the (x',y',z') coordinated gradients and the body axis measurements (x_i, y_i, z_i, i=1,2,3) is required. Noting that the axis of weights, z_i of each of the three gradiometer sensors is inclined at the same angle with respect to z' and that they are equally spaced in azimuth* about z', the following relations can be shown to apply.

$$\gamma_{xz}^{(1)} = 0.4714\gamma_{x'x'} - 0.4714\gamma_{z'z'} + 0.3333\gamma_{y'z'} \quad \text{(C-1a)}$$

$$\gamma_{yz}^{(1)} = 0.5771\gamma_{x'y'} + 0.8165\gamma_{x'z'} \quad \text{(C-1b)}$$

$$\gamma_{xz}^{(2)} = 0.1178\gamma_{x'x'} + 0.3536\gamma_{y'y'} - 0.4714\gamma_{z'z'} - 0.4082\gamma_{x'y'} - 0.1667\gamma_{y'z'} + 0.2887\gamma_{x'z'} \quad \text{(C-1c)}$$

$$\gamma_{yz}^{(2)} = 0.2500\gamma_{x'x'} - 0.2500\gamma_{y'y'} - 0.2887\gamma_{x'y'} - 0.7071\gamma_{y'z'} - 0.4082\gamma_{x'z'} \quad \text{(C-1d)}$$

$$\gamma_{xz}^{(3)} = 0.1178\gamma_{x'x'} + 0.3536\gamma_{y'y'} - 0.4714\gamma_{z'z'} + 0.4082\gamma_{x'y'} - 0.1667\gamma_{y'z'} - 0.2887\gamma_{x'z'} \quad \text{(C-1e)}$$

$$\gamma_{yz}^{(3)} = -0.2500\gamma_{x'x'} + 0.2500\gamma_{y'y'} - 0.2887\gamma_{x'y'} + 0.7071\gamma_{y'z'} - 0.4082\gamma_{x'z'} \quad \text{(C-1f)}$$

where the elements $\gamma_{xz}^{(i)}$ and $\gamma_{yz}^{(i)}$ are the body axis coordinated measurements of the i^{th} sensor and $\gamma_{x'x'}$, $\gamma_{y'y'}$, $\gamma_{z'z'}$, $\gamma_{x'y'}$,

---

*Note that CSDL has designed the cluster to operate with the z' axis vertical.

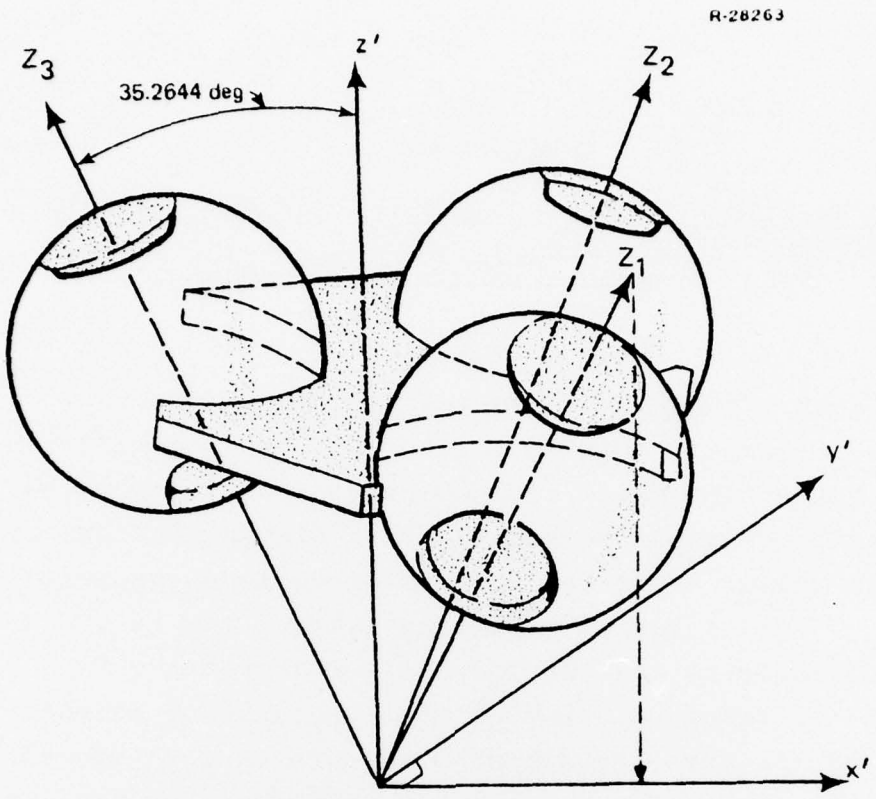

Figure C-1 Three Axis Floated Gradiometer Triad

$\gamma_{y'z'}$, $\gamma_{x'z'}$ are the six elements required to specify the gravity gradient tensor. (Only five are independent).

The system of Eq. C-1 is not of full rank and hence not invertable. However, by use of the Laplace relation as a pseudo measurement, an invertable system can be formulated. The set of Eqs. C-1 is augmented by

$$0 = \gamma_{x'x'} + \gamma_{y'y'} + \gamma_{z'z'} \qquad \text{(C-2)}$$

In matrix notation the augmented system is represented by

$$\underline{z} = H\,\underline{\Gamma} + \text{error} \qquad \text{(C-3)}$$

where

$$\underline{z} = \begin{bmatrix} \gamma_{xz}^{(1)} \\ \gamma_{yz}^{(1)} \\ \gamma_{xz}^{(2)} \\ \gamma_{yz}^{(2)} \\ \gamma_{xz}^{(3)} \\ \gamma_{yz}^{(3)} \\ 0 \end{bmatrix} + \text{error} \qquad \text{(C-4)}$$

$$\underline{\Gamma} = \begin{bmatrix} \gamma_{x'x'} \\ \gamma_{y'y'} \\ \gamma_{z'z'} \\ \gamma_{x'y'} \\ \gamma_{y'z'} \\ \gamma_{x'z'} \end{bmatrix} \qquad \text{(C-5)}$$

and H is the 7×6 coefficient matrix. In similar fashion to Eq. A-8, the least squares solution to Eq. C-3 (when the measurement error vector elements are independent with equal variance) can be written as

$$\hat{\underline{\Gamma}} = H^{\#} \underline{z} \qquad \text{(C-6)}$$

where

$$H^{\#} = (H^T H)^{-1} H^T \qquad \text{(C-7)}$$

Single precision computation of $H^{\#}$ gives

$$H^{\#} = \begin{bmatrix} 1.179 & 0 & -0.236 & 0.333 & -0.236 & -0.333 & 0.333 \\ -0.707 & 0 & 0.707 & -0.333 & 0.707 & 0.333 & 0.333 \\ -0.471 & 0 & -0.471 & 0 & -0.471 & 0 & 0.333 \\ 0 & 0.385 & -0.817 & -0.192 & 0.817 & -0.192 & 0 \\ 0.667 & 0 & -0.333 & -0.471 & -0.333 & 0.471 & 0 \\ 0 & 0.544 & 0.577 & -0.272 & -0.577 & -0.272 & 0 \end{bmatrix} \quad \text{(C-8)}$$

Equation C-6 with $H^{\#}$ as given by Eq. C-8 provides the transformation between gradiometer measurements and the elements of the gravity gradient tensor. It is useful to simplify Eq. C-6 by recognizing that the final element of $\underline{z}$ is zero and deleting the last column of $H^{\#}$. Defining the new quantities $\underline{z}'$ and T as

$$T'(6\times6) = H^{\#} \text{ with last column deleted} \quad \text{(C-9a)}$$

$$\underline{z}'(6\times1) = \underline{z} \text{ with last (zero) element deleted} \quad \text{(C-9b)}$$

The transformation between the six gradiometer measurements and the tensor element estimates is

$$\underline{\Gamma} = T'\underline{z}' \quad \text{(C-10)}$$

The corresponding transformation for covariance quantities is

$$E(\underline{\Gamma}\,\underline{\Gamma}^{T}) = T'\,E(\underline{z}'\underline{z}'^{T})T'^{T} \quad \text{(C-11)}$$

REFERENCES

1. Forward, R.L., et al., "Research Toward Feasibility of an Instrument for Measuring Vertical Gradients of Gravity," Report No. AF 19(628)-6134, Hughes Research Laboratories, Malibu, CA, October 1967.

2. Bell Aerospace, Textron Div., "Gravity Gradiometer Review," Bell Report No. 6324-927001, Fifth Moving-Base Gravity Gradiometer Conference (USAF Academy) January 1977.

3. Charles Stark Draper Laboratory, Inc., "Gradiometer Development Program Interim Report," CSDL Report No. R-1064, April 1977.

4. Forward, R.F. and Ames, C.B., "Prototype Moving Base Rotating Gravity Gradiometer," Fifth Moving-Base Gravity Gradiometer Conference, (USAF Academy) January 1977.

5. Epstein, B., "U.S. Navy Gradiometer Program," Fifth Moving-Base Gravity Gradiometer Conference, (USAF Academy) January 1977.

6. Thomas, S.W. and Heller, W.G., "Efficient Estimation Techniques for Integrated Gravity Data Processing," The Analytic Sciences Corp., Report No. AFGL-TR-76-0232, September 1976.

7. Heller, W.G., "Gradiometer-Aided Inertial Navigation," The Analytic Sciences Corporation, Report No. TR-312-5, January 1975.

8. Gibbons, J.E., Baumgartner, S.L., and Kitahara, R.T., "Air-Mobile Cruise Navigation System Performance Potential (U), Vol. II, Detailed Studies," The Analytic Sciences Corporation, Report No. TR-573-2, January 1977 (SECRET).

9. Gerber, M.A., "Propagation of Gravity Gradiometer Errors in an Airborne Inertial Navigation Systems," AIAA Guidance and Control Conference, (Boston), August 1975.

10. Ames, C.B. et al., "Rotating Gravity Gradiometer," Hughes Research Laboratories, R&D Design Evaluation Report, March 1976.

11. Metzger, E.H., "Summary Error Model-Rotating Accelerometer Gravity Gradiometer," Bell Aerospace Company Report No. 6420-927006, January 1976.

12. Peters, R.C., "Preliminary Gravity Gradiometer Error Models," The Aerospace Corporation, Report No. TOR-0074(4113)-2, June 1974.

13. Lahue, P.M., "Letter Describing Recent RGG Test Results," Hughes Research Laboratories, April 1977.

14. Gelb, A., Ed., Applied Optimal Estimation, MIT Press, Cambridge, 1974.